Reactions ^{58,64}Ni($p,\pi^{\pm}$) at 201 MeV

A. Badalá, R. Barbera, A. Palmeri, G. S. Pappalardo, and A. Bonasera
Istituto Nazionale di Fisica Nucleare, Corso Italia 57, 95129 Catania, Italy

F. Riggi and A. Adorno
Istituto Nazionale di Fisica Nucleare and Dipartimento di Fisica dell'Università di Catania, Corso Italia 57, 95129 Catania, Italy

L. Bimbot
Institut de Physique Nucléaire, Boîte Postale 1, 91406 Orsay CEDEX, France
(Received 8 April 1991)

The production of positive and negative pions induced by 201 MeV protons on ^{58}Ni and ^{64}Ni isotopes has been studied. The double differential cross sections have been measured at the laboratory angles 22°, 35°, 55°, 72°, 90°, 105°, 120°, 138°, 155° and from 20 MeV kinetic energy up to the kinematical limit. Features of the double differential cross sections relative to the two targets are discussed and compared to results obtained at higher incident energies.

PACS number(s): 25.70.−z

I. INTRODUCTION

Pion production at bombarding energy per nucleon below the absolute nucleon-nucleon (NN) threshold is still a puzzling process. It has been studied with light and heavy projectiles in inclusive and exclusive experiments. These reactions are expected to be able to provide information on the mechanisms as well as on nuclear structure [1]. However, in spite of a huge theoretical effort, no model has treated all the involved aspects in a global manner [2–6]. When pion production is induced by heavy ions at intermediate energies, the available energy of the interacting system is high compared to the energy carried out by the outgoing pion and the corresponding phase space for the residual system is very large. On the contrary, the production of pions near the absolute threshold restricts the available final phase space. So for a given interacting system, pion production could be influenced mainly by the effective available energy [7]. Mean-field effects, Fermi motion, Pauli blocking, and transfer of angular momentum play a relevant role. Energy spectra, angular distributions, and total pion yields may be influenced by the discrete and continuum level densities of the residual nuclei. Well known is the importance of the high angular momentum transfer in the production of pions induced by protons [8]. The effect of the large mismatch, between the angular momentum of the incoming proton and that of the outgoing pion, is well discussed in the case of high spin states as calculated [9] for the reaction ^{48}Ca(p,π^-). This mismatch, generally, influences both the absolute probability to populate a given nuclear level of the residual nucleus and the angular distribution of the emitted pion. The continuum pion energy spectra in reactions induced by protons could also be influenced by the impact parameter of the collision. At very low impact parameters, the incoming angular momentum is relatively low, and the matching of angular momenta of the initial and final channels is easily realized. For peripheral collisions a large mismatch occurs. In this case the angular distribution of the pion could be strongly affected.

Pion production at 201 MeV protons has been already studied on other targets [10]. However, in these previous measurements, the isotopic effect was not analyzed, whereas the results from the Indiana University Cyclotron Facility [8,11] (IUCF) relate only to the first 20 MeV of the continuum of residual nuclei.

A review of such studies on Ca isotopes and the $f_{7/2}$ shell nuclei covers only the highest momentum transfer region of the nuclear response function [11]. However since this work is concerned with different isotopes, different incident energies, and different charges of the produced pion, it gives a valuable point of comparison with our results. Results of the present experiment, concerning the nuclei ^{58,64}Ni, will supplement IUCF data [12,13] giving an almost complete angular distribution for pion energies and covering a 40 MeV excitation energy range in the residual nuclei.

The present work is concerned with the production of charged pions in the inclusive ($p,\pi^{\pm}$) reactions at 201 MeV on two Ni isotopes. Preliminary results have been already reported [7]. Here data are discussed and compared with those at higher incident proton energies.

For these two Ni isotopes, the Q value leading to the ground state in a two-body reaction (Q_{gg}) differs strongly in the π^- production process (144 MeV for ^{58}Ni and 133 MeV for ^{64}Ni), whereas the Q values are almost the same for π^+ production (132 MeV for ^{58}Ni and 135 MeV for ^{64}Ni). One should expect this to lead to significant differences in the total cross section values only for negative pions. Then, special attention is given to the total cross section of pion production as a valuable observable for macroscopic considerations. It might also be less sensitive to certain effects, such as Coulomb distortion, nu-

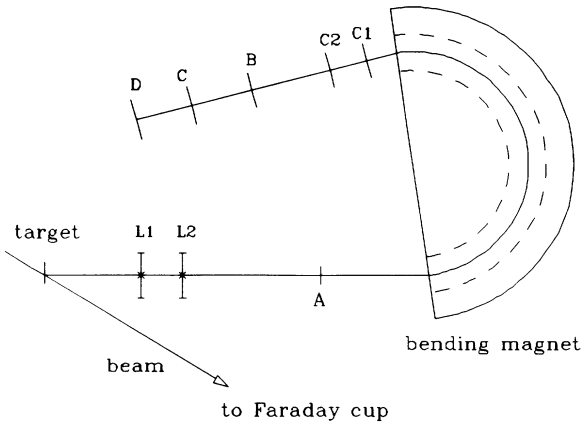

FIG. 1. Setup of the "Mathusalem" spectrometer. $L1$ and $L2$ are the quadrupole lenses used to increase the solid angle of detected pions. $C1$ and $C2$ indicate wire chambers used to detect pion paths in order to reconstruct trajectories and determine the kinetic energy of the pion. Plastic scintillators A, B, C, and D are used for triggering and for time-of-flight measurements.

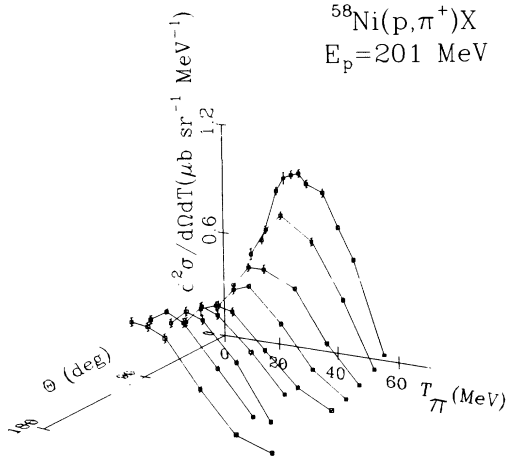

FIG. 2. Double differential cross section $d^2\sigma/d\Omega\,dE$ for the production of positive pions from the ^{58}Ni(p,π^+) reaction at 201 MeV incident energy, as a function of the pion kinetic energy and laboratory angle. The evolution of the positive pion energy spectra from backward to forward angles is clearly shown. Lines connecting points of a given energy spectrum are a guide for the eye.

clear absorption, specific level densities, etc., which would affect differential cross sections and/or angular distributions.

The experiment has been performed by using the 201 MeV proton beam of the Orsay Synchrocyclotron. We have measured double differential cross sections and deduced the total cross sections. The experimental setup is sketched in Fig. 1. Positive and negative pions were detected at 22°, 35°, 55°, 72°, 90°, 105°, 120°, 138°, and 155° in the laboratory system and from an energy of 20 MeV up to the kinematical limit. This large set of values was taken in order to enable a confident extraction of the total cross sections. The target thicknesses were 42.7±0.2 and 41.0±0.2 mg/cm^2, enriched to 99.3% and 98.2% for ^{58}Ni and ^{64}Ni, respectively. The detection of the outgoing charged pions was made with the standard apparatus "Mathusalem," devoted to pion production measurements [7,10]. For a detailed description of the experimental apparatus, see Refs. [7,14].

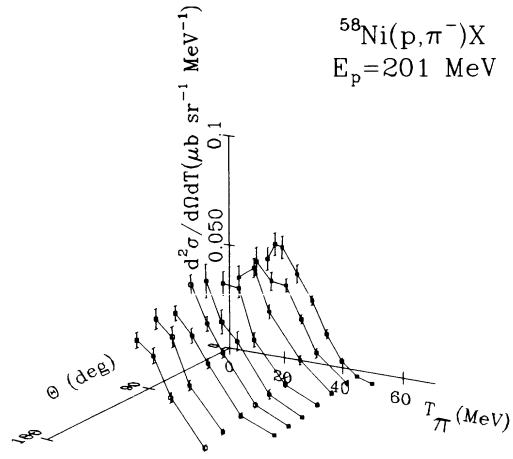

FIG. 3. As in Fig. 2 for negative pions.

II. EXPERIMENTAL RESULTS AND DISCUSSION

A. Energy spectra

Positive and negative pions energy spectra at all detection angles are reported in Figs. 2–5, for the two targets. For a given magnetic field, the double differential cross section has been obtained by taking into account all pions detected in the energy acceptance ΔT of the spectrometer. Then, given values of the double differential cross section are averaged over ΔT and associated with the mean value of the energy in this interval. As a result, any fluctuation in energy spectra disappears. The reported error bars indicate only statistical uncertainty. For the sake of completeness experimental values of the measured double differential cross sections are also reported in Tables I–IV.

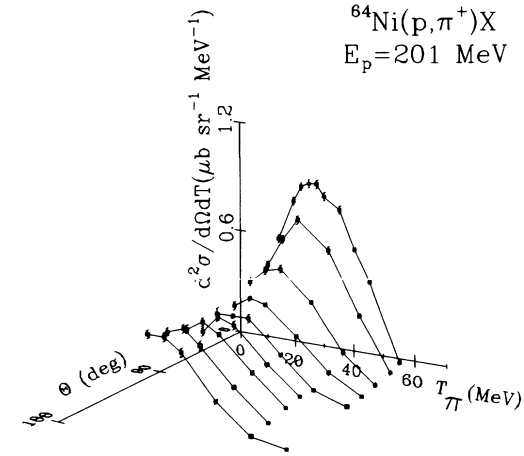

FIG. 4. As in Fig. 2 for the positive pions from the ^{64}Ni(p,π^+) reaction at 201 MeV.

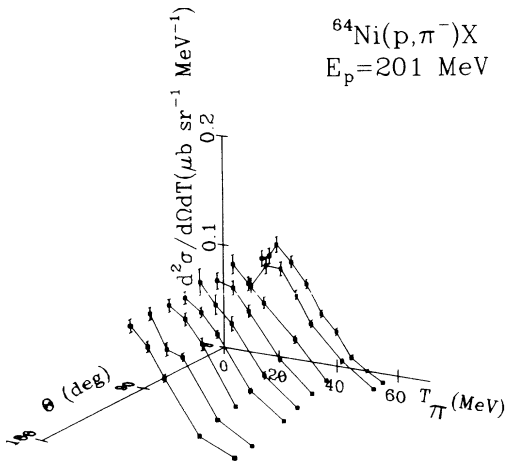

FIG. 5. As in Fig. 4 for negative pions.

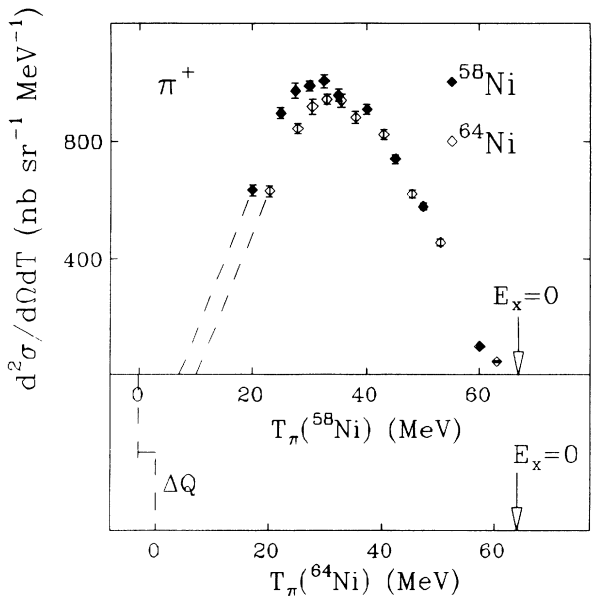

FIG. 6. Energy spectra of positive pions from the ^{58}Ni(p,π^+) (filled diamond, higher-energy scale) and ^{64}Ni(p,π^+) (empty diamond, lower-energy scale) at 22° in the laboratory. The energy spectrum relative to the ^{64}Ni target has been shifted of the ΔQ (see text). The dashed lines give the shape of the extrapolation used to extract total cross sections. For π^+ the low-energy limit is given by the Coulomb barrier.

We first discuss the comparison of positive and negative pion energy spectra, respectively, from the two irradiated targets. Typical energy spectra of charged ions (measured at 22° laboratory) from ^{58}Ni and ^{64}Ni are compared in Figs. 6 and 7. The energy scales are shifted by differences in Q_{gg} in order to compare the shapes and yields of the spectra at the same excitation energy of the residual system (Q_{gg} is the Q value of the two-body reaction in which the pion is emitted). It is evident that the high-energy parts coincide for both isotopes, for a given charge of pion, but the π^+ yield is almost a factor 10 larger than that of π^-. This is also the case for the other angles. The differences which appear in the low-energy pion region are probably due to differences in Q_{gg}. This constrains the falloff to the zero of the cross sections at different excitation energies for the various residual nuclei.

For a given pion charge the shapes of the energy spectra, at the various angles, are similar. For positive pions the maximum of the yield is observed at about 30 MeV and it is slightly shifted at lower energy with the detection angle. This maximum roughly corresponds to one half of the maximum energy at which the pion can be emitted. In reactions induced by protons at higher incident energies [15,16], the positive pion energy spectra show a similar behavior. This feature suggests that the pion production mechanism is similar at low and high incident beam energy. However, because of the relative low energy of pions involved in our measurement, the Coulomb barrier could also play an important role in the falloff of the double differential cross section at the lowest energies. Moreover, the shape of the pion yield near the kinematical limit is due to the level density of the residual nucleus [8,9].

The negative energy spectra show a monotonic decrease with energy, excluding the forward angles where a maximum can be seen between 20 and 25 MeV. Due to the experimental pion energy threshold, no information is

TABLE I. Experimental double differential cross sections for the production of positive pions from the ^{58}Ni(p,π^+) reaction at 201 MeV, as a function of the detection angle (in the laboratory system) and of the pion kinetic energy.

θ \ T_π (MeV)	$d^2\sigma/d\Omega\,dT$ (nb sr^{-1} MeV^{-1}) ^{58}Ni(p,π^+)X									
	20	25	27.5	30	32.5	35	40	45	50	60
22°	634±19	896±18	971±25	988±17	1003±22	955±20	909±18	740±15	578±12	100±4
35°	577±25	718±23		797±21			679±15		402±10	60±4
55°	464±24	558±21		558±19			482±13		221±7	27±2
72°	392±17	481±16		505±14			344±9		133±5	14±2
90°	410±20	444±15		416±14			250±8		92±4	6±1
105°	384±21	473±19		445±16			277±10		103±5	
120°	415±21	480±19		446±16			266±10		96±5	
138°	469±16	524±14		484±16			286±10		89±5	
155°	498±19	492±19		451±16			236±11		63±3	7±2

TABLE II. Experimental cross sections for the production of negative pions from the ^{58}Ni(p,π^-) reaction at 201 MeV, as a function of the detection angle (in the laboratory system) and of the pion kinetic energy.

θ \ T_π (MeV)	$d^2\sigma/d\Omega\,dT$ (nb sr^{-1} MeV^{-1}) ^{58}Ni$(p,\pi^-)X$							
	20	22.5	25	30	35	40	45	50
22°	50±5	57±5	56±5	45±4	34±2	20±2	9±1	3±1
35°	51±6		43±4	42±3	28±2	14±2		3±1
55°	47±5		52±4	34±3		15±2		3±1
72°	47±5		46±4	25±3		8±1		2±1
90°	51±7		35±5	28±4		8±2		1±1
105°	52±4		37±3	26±2		7±1		1±1
120°	43±3		35±3	25±2		6±1		1±1
138°	44±4		38±4	20±2		4±1		
155°	39±3		34±3	19±2		2±1		

available on the spectral shape at energies lower than 20 MeV. Data at higher incident energy [15,16] show that negative pion spectra are less hard than the positive ones. Moreover, for a given target, at the same detection angle, the maximum in the negative pion spectrum is located at lower energy relative to the positive one. This effect is also observed for the two studied targets.

The energy shift between the two maxima, observed at 22°, is roughly 8 MeV. The origin of this shift is not clearly understood. It could be attributed to Coulomb effects but, at higher incident energies, positive and negative pion energy spectra show a very large shift (about 100 MeV) [15,16] which is not compatible with a Coulomb distortion.

B. Angular distributions

The angular distributions of the positive and negative pions, in the laboratory system, for the ^{58}Ni target, are shown in Figs. 8 and 9, respectively. Data concerning the ^{64}Ni target are shown in Figs. 10 and 11. The angular distributions of positive pions are forward peaked with only a light enhancement at backward angles. The angular distribution of the negative ones is almost flat with a light decrease with angle. These trends are also observed for the ^{64}Ni target, suggesting that the mechanism of pion production is insensitive to the nuclear structure of the target nuclei, as isospin and/or shell effects. In order to study in more detail this angular behavior, in Figs. 12–15 the angular distributions for different pion energies are shown for the two charge states and for the two targets. The energy bin of pions reported in each figure corresponds to the $\Delta p/p = \pm 2.5\%$ acceptance of the spectrometer.

The angular distributions obtained for 20, 30, 40, and 50 MeV pions disentangle the origin of the peak at forward angles. Low-energy pions, for both targets, show an angular distribution symmetric around 90° with a minimum of the positive pions at this angle. With the increasing pion energy more and more contributions occur at forward angles. It is evident that the main contribution to the forward yield in the energy integrated angular distribution of Figs. 8 and 10 comes from the most energetic positive pions, because of their large yields compared to the low-energy ones. A similar behavior appears in the angular distributions of the negative pions.

This forward peaked distribution was also observed in Ref. 11 for ^{48}Ca(p,π^-). The variation of the shape of the angular distribution with pion energy is a new experimental results that may have several origins. The strong forward peak of π^+ production at the beginning of the continuum, i.e., in a region of low level density, suggests an

TABLE III. Experimental cross sections for the production of positive pions from the ^{64}Ni(p,π^+) reaction at 201 MeV, as a function of the detection angle (in the laboratory system) and of the pion kinetic energy.

θ \ T_π (MeV)	$d^2\sigma/d\Omega\,dT$ (nb sr^{-1} MeV^{-1}) ^{64}Ni$(p,\pi^+)X$									
	20	25	27.5	30	32.5	35	40	45	50	60
22°	631±19	844±18	917±25	941±17	938±22	881±20	822±17	622±14	455±11	47±3
35°	512±24	657±23		768±21			635±15		306±9	28±2
55°	456±24	527±20		547±18			396±12		157±6	16±2
72°	371±17	421±15		397±12			261±8		96±4	10±2
90°	372±17	373±14		367±12			210±8		63±3	7±2
105°	312±20	397±19		372±16			192±9		70±5	
120°	359±21	409±19		361±15			200±9		61±4	
138°	388±16	420±19		354±15			184±9		44±4	
155°	417±16	417±19		365±15			155±8		31±2	5±2

TABLE IV. Experimental cross sections for the production of negative pions from the $^{64}Ni(p,\pi^-)$ reaction at 201 MeV, as a function of the detection angle (in the laboratory system) and of the pion kinetic energy.

θ \ T_π (MeV)	$d^2\sigma/d\Omega\,dT$ (nb sr^{-1} MeV^{-1}) $^{64}Ni(p,\pi^-)X$							
	20	22.5	25	30	35	40	45	50
22°	100±7	103±7	114±8	100±5	82±4	57±3	47±3	22±2
35°	79±7		99±7	98±6	77±4	53±3		24±1
55°	105±8		90±6	75±5		47±3		16±1
72°	96±8		92±6	74±5		37±2		12±1
90°	101±11		84±8	70±6		31±3		9±1
105°	93±5		83±4	67±3		25±2		5±1
120°	92±5		83±5	65±5		19±1		
138°	92±5		66±5	62±3		17±1		2±1
155°	89±5		75±4	53±2		13±1		2±1

interaction of the incoming proton with surface nucleons of the target nucleus. For peripheral collisions outer nucleons are involved and the probability to create an energetic pion is higher because scattered nucleons can generate low-lying final state. In this case, moreover, a large mismatch of the angular momentum, between the incoming proton and the outgoing pion, occurs and angular distributions can be strongly affected by angular momentum conservation.

On the other hand, the symmetry around 90° of the angular distributions of the low-energy pions, which correspond to a very high excitation energy, could be explained by an interaction of the incoming proton with many nucleons of the target. Let us consider one collision at very low impact parameter. For collisions of the incident proton with a nucleon of the inner shell, only a low-energy pion can be produced because of the high binding energy and the necessity for the scattered nucleons to go into available states. In this case the residual nucleus gets a high excitation energy and the available energy for the pion is very low. Because of the low impact parameter no mismatch of the incoming proton and outgoing pion angular momenta occurs. So, the angular distribution could be seen as the consequence of only low partial wave numbers contribution.

C. Total cross sections

Total cross sections are obtained from a double integration over angle and energy (after an energy extrapolation following the dashed lines of Fig. 6 and Fig. 7). As

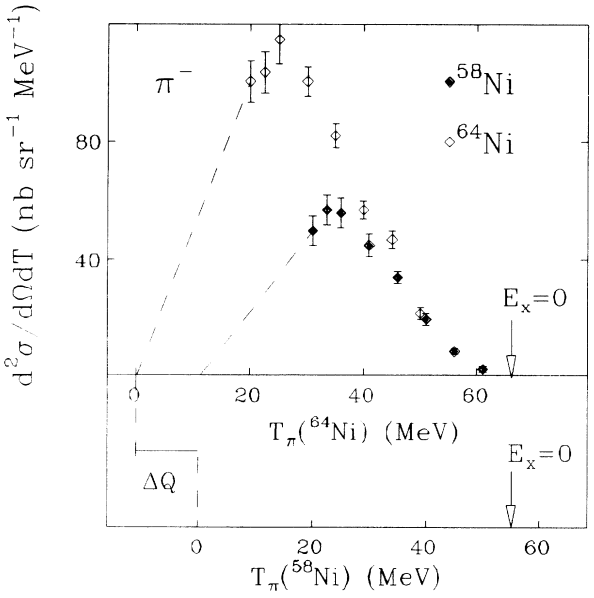

FIG. 7. Energy spectra of negative pions from the $^{58}Ni(p,\pi^-)$ (filled diamond, lower-energy scale) and $^{64}Ni(p,\pi^-)$ (empty diamond, higher energy scale) at 22° in the laboratory. The energy spectrum relative to the ^{58}Ni target has been shifted of the ΔQ.

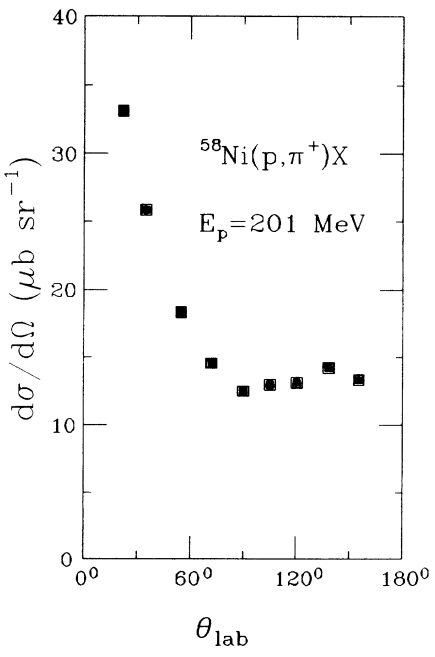

FIG. 8. Angular distribution, in the laboratory frame, of positive pions from the $^{58}Ni(p,\pi^+)$ reaction at 201 MeV proton energy. At each angle, the double differential cross section is integrated in the energy range starting from the extrapolated low-energy limit.

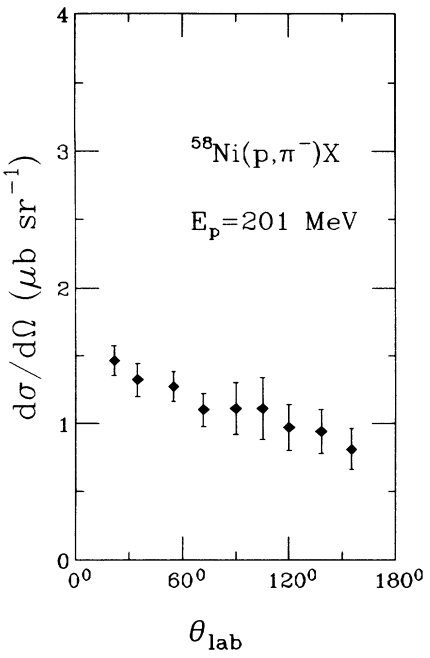

FIG. 9. As in Fig. 8, for negative pions.

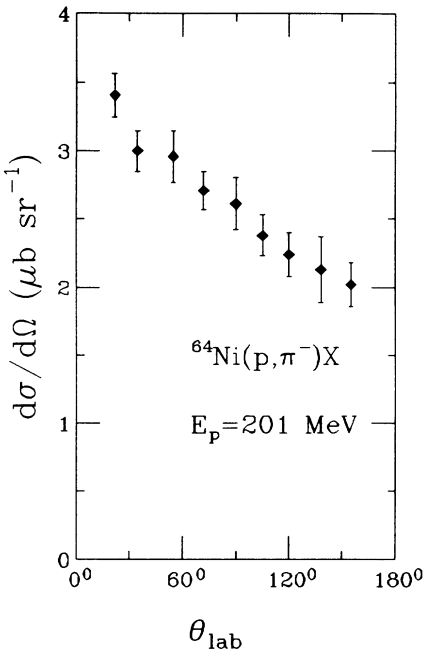

FIG. 11. As in Fig. 10, for negative pions.

a consequence, the integrated total cross sections cover different energy ranges due to the different kinematical limits. Obtained values are given in Table V.

These total cross sections vary in the same sense as Q_{gg} but a direct relationship cannot be established from this limited set of values. Part of the variation comes from the different energy range over which the integration is done, but other effects could play a role. Throwe *et al.* [11] attempted to relate the yield of π^- in the first 20 MeV excitation of the continuum to the occupancy numbers in the $f_{7/2}$ shell. The calculation of Scholten and Toki [6], using the two-particle–one-hole ($2p$-$1h$) state density, in a Fermi gas, for the ^{42}Ca and ^{48}Ca isotopes, works within a factor of 2. Before concluding this section we must point out a striking feature of our results as compared to the IUCF measurements. For (p,π^-) on ^{42}Ca and ^{48}Ca in the first 20 MeV of the excitation energy region at 30°, a yield ratio (^{48}Ca/^{42}Ca) of 2 was obtained [11]. This was attributed to Pauli blocking and neutron excess at the surface. In our experiment the absolute values of the cross section for the first 20 MeV region of the continuum are identical at each angle for both Ni isotopes though, of course, our measurements are concerned with a different shell and structure effects cannot be excluded.

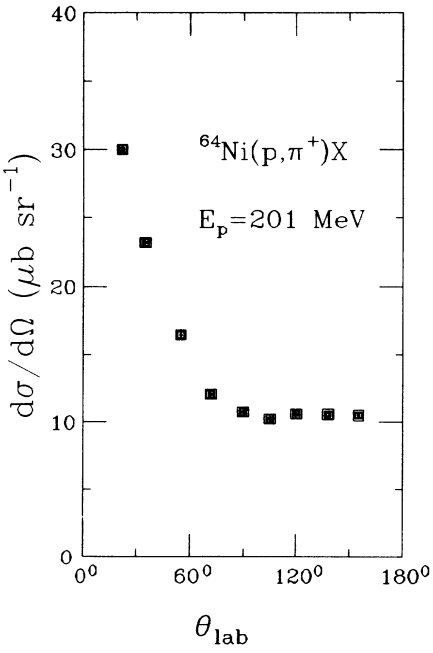

FIG. 10. Angular distribution, in the laboratory frame, of positive pions from the ^{64}Ni(p,π^+) reaction at 201 MeV proton energy.

In Fig. 16 the total cross sections of the irradiated targets are reported together to the data of Ref. [10] as a function of the target mass A. An almost flat distribution is observed for positive pion total cross section for

TABLE V. Experimental total cross sections for the charged pion production induced by 201 MeV protons on ^{58}Ni and ^{64}Ni. Q_{gg} is the Q value of the two-body reaction, when the residual nucleus lies at the ground state. Values are obtained after the extrapolation of the energy spectra, as shown in Figs. 6 and 7.

Reaction	σ_{exp} (μb)	Q_{gg} (MeV)
^{58}Ni(p,π^+)X	200±10	−132
^{64}Ni(p,π^+)X	170±8	−135
^{58}Ni(p,π^-)X	16±2	−144
^{64}Ni(p,π^-)X	34±3	−133

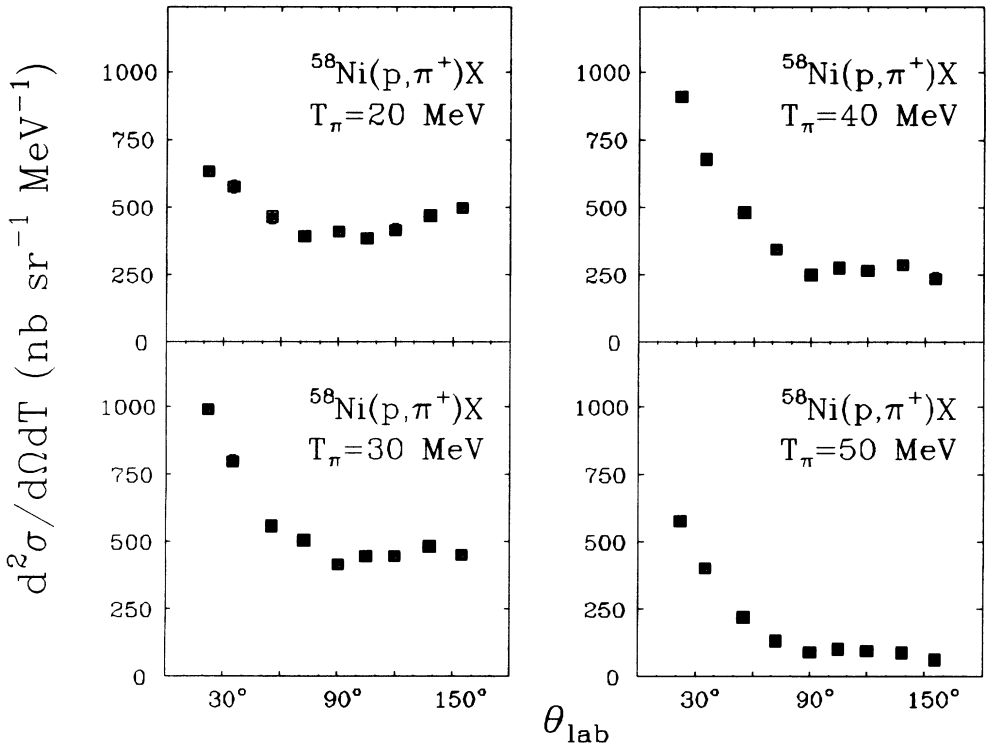

FIG. 12. Angular distributions of positive pions from the reaction ^{58}Ni(p,π^+) at 201 MeV, for various energies of the pions.

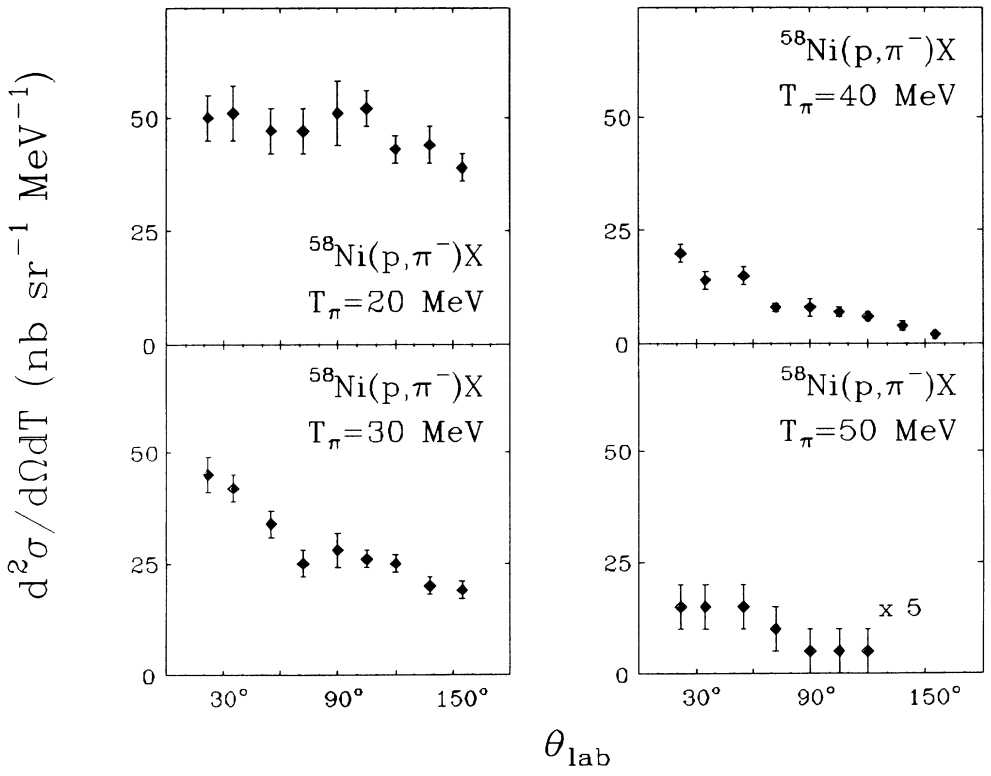

FIG. 13. Angular distributions of negative pions from the reaction ^{58}Ni(p,π^-) at 201 MeV, for various energies of the pions.

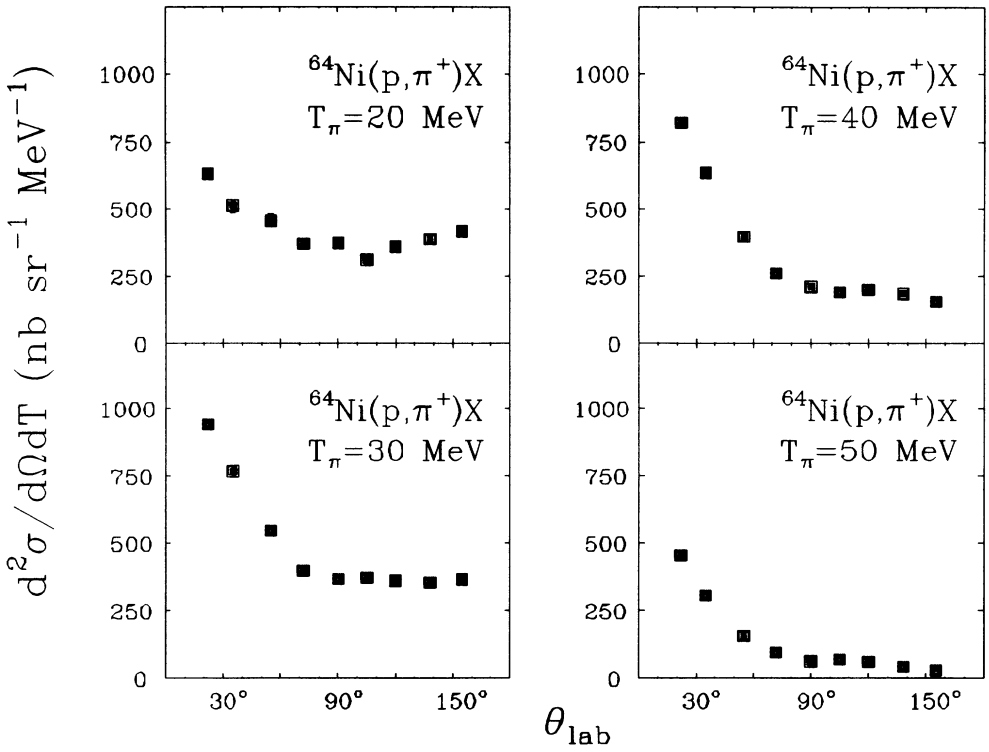

FIG. 14. Angular distributions of positive pions from the reaction ^{64}Ni(p,π^+) at 201 MeV, for various energies of the pions.

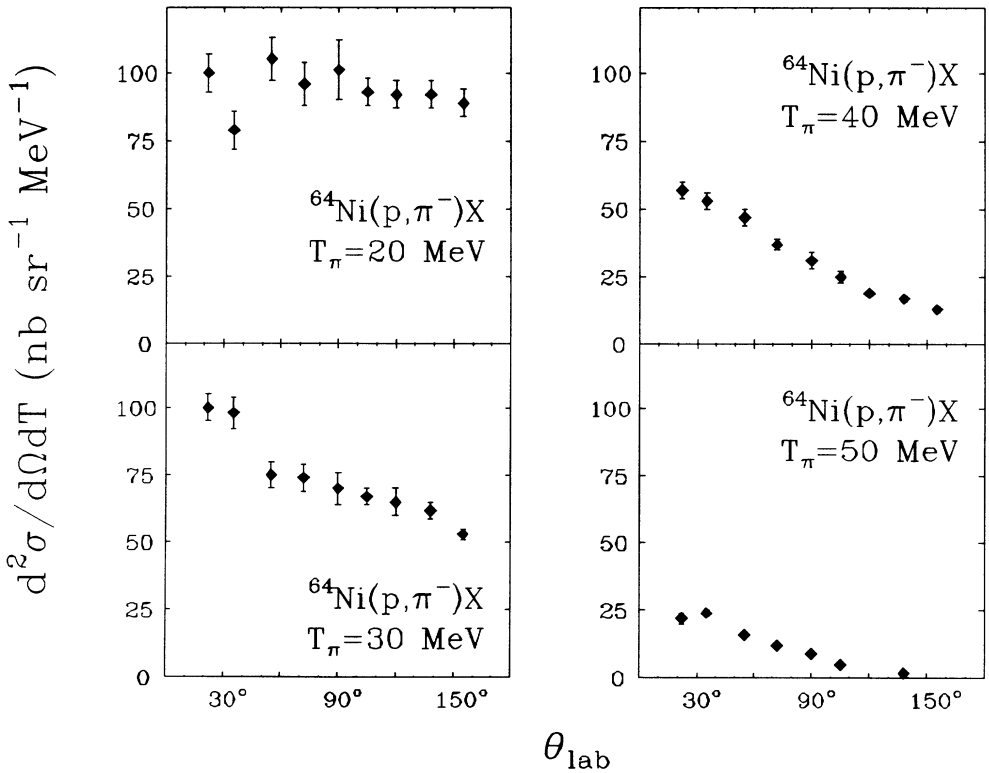

FIG. 15. Angular distributions of negative pions from the reaction ^{64}Ni(p,π^-) at 201 MeV, for various energies of the pions.

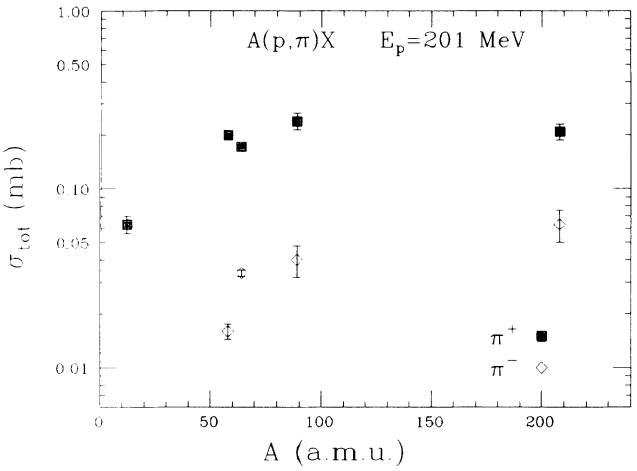

FIG. 16. Total cross section of positive (filled square) and negative (empty diamond) pions versus the target mass, for 201 MeV incident protons. Data relative to ^{12}C, ^{89}Y, and ^{nat}Pb are taken from Ref. [10].

mass greater than $A=12$. This saturation effect can be partially attributed to the reabsorption of the created pion. Moreover, the increased Coulomb potential for heavier nuclei acts twofold in lowering the total yield: the repulsion in the incoming channel which subtracts a fraction of the kinetic energy to the incident proton and the Coulomb barrier acting on the outgoing positive pion with a suppression of a part of low energy pion yield. Negative pions are not affected by this last effect and data exhibit a slight increase with the target mass. Unfortunately no calculations exist which take into account such effects and the conclusions remain qualitative.

At higher bombarding energies many authors compare the total cross sections [15–17] and angle integrated pion momentum distributions [17] to the predictions of the intranuclear cascade approach [18] and related models [19]. These cascade Monte Carlo calculations are based on the on-shell incoherent hadron-hadron collision and the produced pion can be reabsorbed or exchange its charge. The resulting σ_{tot} follows the law $Z^{2/3}$ and $N^{1/3}$ for positive and negative pions, respectively [19].

D. The π^+ to π^- ratio

In Table VI the π^+ to π^- ratio is reported for all detection angles and measured kinetic energies only for the ^{64}Ni target because of the same energy range for positive and negative pions. For all kinetic energies π^+/π^- ratio shows a minimum at 90° with a low increase going away from this angle and a more pronounced maximum at forward angles for all energies. A similar behavior can be deduced from data of Ref. [10] relative to the Y and Pb targets for which no Q-values differences exist between positive and negative pions.

The angular and energy dependence of the π^+ to π^- ratio has also been deduced from data at 730 MeV [16] and it is reported in parenthesis in Table VI. Comparison with data at 201 MeV cannot be done in a straightforward manner because of the large differences in the pion energy dynamics. However, in order to reduce space phase effects the extracted values have been calculated as a function of the fraction $\epsilon=T_\pi/T_{max}$ of the pion kinetic energy T_π to the maximum allowed kinetic energy T_{max}.

The π^+ to π^- ratio distribution at 730 MeV does not differ substantially from that extracted at 201 MeV. Forward angles and higher energies present the highest values, but the valley observed at 201 MeV is not evident. However, a complete satisfactory comparison is not possible because the yield of high energy pions at backward angles is not reported at 730 MeV and very low energy pions have not been measured in our experiment.

The experimental ratio $R=\sigma(\pi^+)/\sigma(\pi^-)$ of the positive to negative total cross section is about 5 for the ^{64}Ni. R is 12.5 for the ^{58}Ni target but this high value can be attributed to the large π^- suppression due to the high negative Q value compared to the π^+ case.

R value systematics between 180 and 730 MeV are reported in Table VII for various irradiated targets. The R^{-1} $[=\sigma(\pi^-)/\sigma(\pi^+)]$ is also reported for pion production induced by the neutron beam at 600 MeV [20]. Induced charged pion production has been studied at lower neutron incident energy [21] but no pion charge separation has been performed. For all target masses a decrease of the R value with the proton incident energy is observed. R saturates between 600 and 730 MeV for light

TABLE VI. The ratio $d^2\sigma(\pi^+)/d^2\sigma(\pi^-)$ of the double differential cross section at each detection angle and at each measured kinetic energy. The parameter ϵ represents the ratio of the kinetic energy T_π to the maximum allowed kinetic energy T_{max}. Data at 730 MeV are from Ref. [16] and are relative to the Cu target.

	$R=d^2\sigma(\pi^+)/d^2\sigma(\pi^-)$										^{64}Ni(p,π)
ϵ / θ	(0.18)	0.31	(0.35)	0.39	(0.43)	0.47	(0.60)	0.63	(0.69)	0.78	(0.82)
22°	(3.1)	6.3	(4.5)	7.4	(5.7)	9.4	(9.5)	15.4	(11.5)	20.7	(13.8)
35°	(3.4)	6.5	(4.8)	6.6	(5.8)	7.8	(8.0)	12	(1.5)	12.7	(10.3)
55°	(3.8)	4.3	(4.9)	5.9	(5.3)	7.3	(7.1)	8.4	(7.0)	9.8	
72°	(3.9)	3.9	(5.0)	4.6	(5.1)	5.4	(4.7)	7.1		8	
90°	(4.3)	3.7	(4.8)	4.4	(4.5)	5.2		6.8		7	
105°	(4.4)	3.4	(5.6)	4.8	(5.5)	5.6		7.7		15	
120°	(4.7)	3.9	(5.6)	4.9	(4.0)	5.6		10.5			
135°	(4.6)	4.2	(5.2)	6.4	(2.7)	5.7		10.8		21	
155°	(4.8)	4.7	(5.1)	5.6	(4.0)	6.9		11.9		15.5	

TABLE VII. The ratio $R=\sigma(\pi^+)/\sigma(\pi^-)$ is given for many targets at various incident proton energies. Data relative to a 600 MeV neutron beam are indicated by a superscript a and reported R values are calculated as the π^- to π^+ yields. The ratio R, at the energies other than 201 MeV, in the column of the ^{64}Ni, are relative to Cu targets. R values at 585 MeV have been deduced from data of Ref. [15]. R values at 730 MeV have been deduced from data of Ref. [16].

	$R=\sigma(\pi^+)/\sigma(\pi^-)$ Target				
	^{12}C	^{58}Ni	^{64}Ni	^{89}Y	^{nat}Pb
E_p (MeV)	$R^{elem}=11$	10.3	8.6	8.6	7.2
180				7.8±3	6.0±2.2
201		12.5±1.7	5.0±0.5	6.0±1.3	3.3±0.8
300	10±2				2.0±0.2
400	8.0±1				2.0±0.1
500	7.5±1				2.1±0.1
585	6.1±1	4.2±0.7	3.3±0.6		2.1±0.4
730	5.3±0.4		3.1±0.3		1.9±0.2
600[a]	5.9±0.5 [a]		5.4±0.2 [a]		7.4±1.0 [a]

[a] $R^{-1}=\sigma(\pi^-)/\sigma(\pi^+)$. Data are relative to 600 MeV bombarding neutrons [20].

targets and at lower bombarding energies for heavier targets.

The R ratio could be related to the isospin effect of the elementary processes $NN\rightarrow NN\pi^{\pm}$ if one does not take into account charge dependence of the rescattering effects such as reabsorption or charge exchange of the pion.

In the following R^{elem} will indicate the π^+ to π^- ratio calculated by taking into account the elementary collision cross sections $[\sigma(pp\rightarrow pn\pi^+)\simeq 10\sigma(pn\rightarrow pp\pi^-$ or $nn\pi^+)]$ and in the hypothesis that only the first collision between the incoming proton and a nucleon of the target produces a pion ("first chance" picture [10]). In Table VII, R^{elem} is reported as a reference for various targets. It is simply calculated as the ratio of the proton neutron numbers of the target multiplied by the ratio $[\sigma(pp\rightarrow pn\pi^+)+\sigma(pn\rightarrow pn\pi^+)]/\sigma(pn\rightarrow pn\pi^-)$.

Secondary NN collisions can strongly modify this ratio. In fact, if one assumes that first collisions proton-neutron undergoes secondary neutron-neutron collisions which produce negative pions with a cross section one order of magnitude greater than the proton-neutron collision, the π^+ to π^- ratio becomes lower than R^{elem}.

R^{elem} is around 9 for the ^{64}Ni but 10% of secondary collision reduces to 5 the π^+ to π^- ratio.

Also the level densities of the two residual nuclei (i.e., ^{65}Ni and ^{65}Zn) could play a significant role to determine the π^+ to π^- ratio . It is stated in Ref. [11] that the ratio of π^+ to π^- production has the same value ($\simeq 10$) in the continuum measurement for ^{48}Ti(p,π^+) and ^{48}Ca(p,π^-), as for the elementary N-N interaction. Since the two reactions lead to the same final nucleus, the ^{49}Ti, the final state effects can be considered absent and this ratio is therefore attributed to an isospin effect.

For ^{12}C, the experimental R value is 10 at 300 MeV (no data exist at lower energies) and $\simeq 6$ at the highest bombarding energies. Intranuclear cascade calculations reproduce well the experimental R value at high bombarding energies but underestimate this ratio at 300 MeV [17]. The disagreement at lower bombarding energies can be due to the difference in the Q value for the two charged pions (-136 and -158 MeV for positive and negative pions, respectively). This large Q-value difference could also explain the very low (not measured) cross section of negative pions at 201 MeV [10]. With increasing the bombarding energy, Q-values differences play a minor role and the intranuclear cascade calculations well account for the experimental R values [17]. Moreover for 585 MeV proton and 600 MeV neutrons R and R^{-1} have the same value at variance with the other targets. The ^{12}C result can then be explained as due to the same number of neutrons and protons of the target. In this case the decreasing of R with the incident energy could be due essentially to the secondary nucleon-nucleon collisions.

Data on ^{58}Ni at 585 MeV have been recently [22] compared with a good agreement to INC calculations. The 201 MeV R value (12.5) is larger than the expected R^{elem} ($\simeq 10$). This very large R value is due, as already discussed, to the strong suppression of the π^- because of the high negative Q value and cannot be explained quantitatively without a well established relation between total cross section and Q value.

For the ^{64}Ni, R decreases with the incident energy going from 5 at 201 MeV to 3 at 730 MeV and R^{-1}, relative to the neutron beam data, is very different from R at 585 MeV. Indeed, for the Ni target, the neutron excess at the nuclear surface can enhance the negative pion yield.

The neutron excess at the nuclear surface could be at the origin of the large difference observed between R and R^{-1} for the Pb target. For this target, at the lowest bombarding energy ($E_p=180$ MeV), the experimental R value (6.0) approaches R^{elem}. However this evidence does not mean that the NN scattering dominates the total cross section at so low incident energy, though the hypothesis that only first chance collisions produce pions seems reasonable because of the low available energy in the collision. At 201 MeV the R value goes down to 3.3. We observe that energy spectra of positive and negative pions differ not so much and it is very hard to attribute this strong change of R to variations in the reabsorption pro-

cess with the charge state of the pion. It seems more simple to attribute the R variation to the onset of some secondary NN collisions which enhance negative pion yield.

The same behavior, as in the Pb case, is observed for the ^{89}Y target. We observe that for both Y and Pb targets there is no difference in Q values between positive and negative pions.

III. CALCULATIONS

In Ref. [10] the pion production from proton-nucleus collisions as a function of the bombarding energy has been calculated in the frame of a first chance nucleon-nucleon model. Reported results are compared to the measured total cross sections at 201 MeV protons and large discrepancies are observed. In particular negative pion yields are underestimated by an order of magnitude and no pion energy spectra have been calculated. In order to get a better understanding of the process which determines pion production in proton-nucleus collisions, we performed a microscopic Boltzmann-Nordheim-Vlasov (BNV) calculation [23], for a comparison with the experimental double differential cross sections. Such calculations have recently been applied, quite successfully [24], to the production of low energy pions by heavy ion collision.

We would like to stress that for proton-nucleus pion production, near the absolute threshold, the BNV calculation gives just a rough description of the process since the π leaves the nucleus with almost no excitation energy and, therefore, a detailed quantum mechanical description of the initial and final nuclei is needed. However, as opposed to the first chance model, the performed BNV calculations take automatically into account secondary collisions which, in principle, enhance the negative pion yield more than the positive one.

Because of the experimental forward large enhancement of positive pion yields, BNV calculations have been performed only at large detection angles where positive and negative pion yields do not show large differences.

The equation was numerically solved by using the test particles method [25], i.e., expressing the phase space as a collection of $N(1+A)$ test particles. A is the target mass number and N is a number large enough in order to get a smooth distribution function and convergent numerical results. For π production, since the yield is very low, we needed an accurate numerical precision and we used a total test particle number equal to 50 000. The time evolution of the test particles was followed through the Hamiltonian equation of motion with a Skyrme mean field, giving $K=225$ MeV compressibility, using a time step $\Delta T=0.5$ fm/c. The target nucleus is given at time $T=0$ fm/c by a Fermi gas, with a Fermi momentum $P_F=238$ MeV/c and a radius equal to $1.2A^{1/3}$. Of course the results are somewhat dependent on the value of the used P_F, but we did not try to change it to better fit the data. The collision integral was simulated by the mean free path [26] and the elementary NN cross section was assumed 40 mb. The pion production was calculated perturbatively following Ref. [23] using the elementary cross section given in Ref. [27].

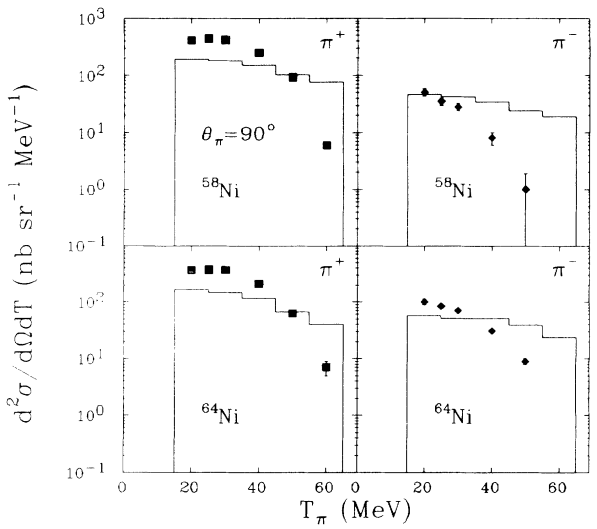

FIG. 17. Energy spectra at 90° of positive (left side) and negative (right side) pions form the reaction ^{58}Ni$(p,\pi^{\pm})$ (up) and ^{64}Ni$(p,\pi^{\pm})$ (down) at 201 MeV. Histograms indicate double differential cross sections calculated by the model presented in the text. For experimental yields error bars are statistical fluctuations.

In Fig. 17 we compare calculations (histograms) with the experimental double differential cross sections at 90° for both Ni isotopes and for π^+ and π^-. At low pion energies calculations reproduce data within a factor of two. Yields of high energy pions are largely overestimated as expected because the level densities of the residual nuclei are not accounted for by the used model. The calculated energy spectrum of negative pions from the ^{58}Ni overestimates the experimental one in all the energy range, probably because of the already discussed effect due to the Q value of the reaction. We observe that calculations have been performed without taking into account differences in the available total energy for both targets and charge of the pions.

IV. CONCLUSIONS

The two isotopes ^{58}Ni and ^{64}Ni have been irradiated by 201 MeV protons for the study of the charged pion production. Angular and energy differential cross sections have been measured in wide ranges allowing for a good estimate of the total cross sections. Data are in good agreement with previous measurement at the same incident energy and confirm a saturation of the σ_{tot} with the target mass which can be due to the reabsorption of the pion and to the Coulomb field acting on both the incoming and outgoing channel. The only observed difference between the two targets concerns the ratio of total yields of positive to negative pions which reflects the different allowed final phase space strongly dominated by the Q value in a two-body reaction.

The angular distributions of pions are strongly dependent on the pion kinetic energy with a forward peaking for the most energetic pions. Positive pions, compared to the negative ones, show a large forward contribution for

both targets showing that this effect is independent of the nuclear structure of the target.

The ratio of positive to negative pion yield, as a function of the kinetic energy and the emission angle, show a slight symmetry around 90° which is not found at 730 MeV.

Comparison with experimental data at higher incident energies has been made by studying the ratio of positive to negative pion yields. This ratio decreases with the incident energy of the proton and its maximum value is found near the absolute threshold approaching the elementary nucleon-nucleon pion production cross section ratio.

At this relatively low incident energy mean-field effects, such as Fermi motion and Pauli blocking, could dominate the pion yield. Reliable calculations are needed in order to understand the main features of the pion production at energy very near the absolute threshold.

[1] H. C. Wolfe, in *Pion Production and Absorption in Nuclei* (Bloomington, Indiana, 1981), Proceedings of the Conference on Pion Production and Absorption in Nuclei, edited by Robert Bent, AIP Conf. Proc. No. 79 (AIP, New York, 1982); B. Hölstad, Adv. Nucl. Phys. **11**, 135 (1979); H. W. Fearring, Prog. Part. Nucl. Phys. **7**, 113 (1981).
[2] G. F. Bertsch, Phys. Rev. C **15**, 713 (1977).
[3] D. Vasak, B. Muller, and W. Greiner, Phys. Scr. **22**, 25 (1980).
[4] R. Shyam and J. Knoll, Nucl. Phys. **A426**, 606 (1984).
[5] M. Prakash, P. Braun-Munzinger, and J. Stachel, Phys. Rev. C **33**, 937 (1986).
[6] O. Scholten and H. Toki, Phys. Rev. C **34**, 601 (1987).
[7] A. Palmeri, S. Aiello, A. Badalá, R. Barbera, G. S. Pappalardo, L. Bimbot, F. Reide, N. Willis, and H. Oeschler, Phys. Rev. C **40**, 1081 (1989).
[8] S. E. Vigdor, T. G. Throwe, M. C. Green, W. W. Jacobs, R. D. Bent, J. J. Kehayas, W. K. Pitts, and T. E. Ward, Phys. Rev. Lett. **49**, 1314 (1982).
[9] B. A. Brown, O. Scholten, and H. Toki, Phys. Rev. Lett. **51**, 1952 (1983).
[10] L. Bimbot *et al.*, Nucl. Phys. **A440**, 636 (1985).
[11] T. G. Throwe, S. E. Vigdor, W. W. Jacobs, M. C. Green, C. W. Glover, T. E. Ward, and B. P. Hichwa, Phys. Rev. C **35**, 1083 (1987).
[12] J. J. Kehayias, R. D. Bent, M. C. Green, M. A. Pickar, and R. E. Pollock, Phys. Rev. C **33**, 725 (1986).
[13] H. P. Pile, R. D. Bent, R. E. Pollock, P. T. Debevec, R. E. Marrs, M. C. Green, T. P. Sjoreen, and F. Soga, Phys. Rev. Lett. **42**, 1461 (1979).
[14] N. Willis, L. Bimbot, N. Koori, Y. Le Bornec, F. Reide, A. Willis, and C. Wilkin, J. Phys. G **7**, L195 (1981); Y. Le Bornec *et al.*, Phys. Rev. Lett. **47**, 1870 (1981); L. Bimbot *et al.*, Phys. Rev. C **30**, 739 (1984); B. Million *et al.*, Nucl. Phys. **A459**, 594 (1986).
[15] J. F. Crawford *et al.*, Phys. Rev. C **22**, 1184 (1980).
[16] D. R. F. Cochran, P. N. Dean, P. A. M. Gram, E. A. Knapp, E. R. Martin, D. E. Nagle, R. B. Perkins, W. J. Shlaer, H. A. Thiessen, and E. D. Theriot, Phys. Rev. D **6**, 3085 (1972).
[17] N. J. Di Giacomo, M. R. Clover, R. M. De Vries, J. C. Dousse, J. S. Kapustinsky, P. L. McGaughey, W. E. Sondheim, W. S. Sunier, M. Buenerd, and D. Lebrun, Phys. Rev. C **31**, 292 (1985).
[18] K. Chen, G. Friedlander, G. D. Harp, and J. M. Miller, Phys. Rev. C **4**, 2234 (1971); G. D. Harp, *ibid.* **10**, 2387 (1974); Y. Yariv and Z. Fraenkel, *ibid.* **24**, 488 (1981).
[19] R. R. Silbar and M. M. Sternheim, Phys. Rev. C **8**, 492 (1973); M. Sternheim and R. Silbar, Phys. Rev. D **6**, 3117 (1972).
[20] K. O. Oganesyan, Zh. Eksp. Teor. Fiz. **54**, 1273 (1968) [Sov. Phys. JETP **27**, 679 (1968)].
[21] R. Büchle *et al.*, Nucl. Phys. **A515**, 541 (1990).
[22] H. Friedemann, Institut Für Kernphysik Technische Hochschule (Darmstadt), Diplomarbeit (1989) unpublished.
[23] A. Bonasera, G. Russo, and H. H. Walter, Phys. Lett. B **266**, 337 (1990).
[24] A. Badalá *et al.*, Phys. Rev. C **43**, 190 (1991).
[25] G. Bertsch and S. Das Gupta, Phys. Rep. **160**, 190 (1988).
[26] A. Bonasera, G. F. Burgio, and M. Di Toro, Phys. Lett. B **221**, 233 (1989).
[27] B. J. Ver West and R. A. Arndt, Phys. Rev. C **25**, 1979 (1982).